

Design of non-diagonal stiffness matrix for assembly task

Tsukasa Kusakabe¹, Sho Sakaino² and Toshiaki Tsuji¹

Abstract—Compliance control is an increasingly employed technique used in the robotic field. It is known that various mechanical properties can be reproduced depending on the design of the stiffness matrix, but the design theory that takes advantage of this high degree of design freedom has not been elucidated. This paper, therefore, discusses the non-diagonal elements of the stiffness matrix. We proposed a design method according to the conditions required for achieving stable motion. Additionally, we analyzed the displacement induced by the non-diagonal elements in response to an external force and found that to obtain stable contact with a symmetric matrix, the matrix should be positive definite, i.e., all eigenvalues must be positive, however its parameter design is complicated. In this study, we focused on the use of asymmetric matrices in compliance control and showed that the design of eigenvalues can be simplified by using a triangular matrix. This approach expands the range of the stiffness design and enhances the ability of the compliance control to induce motion. We conducted experiments using the stiffness matrix and confirmed that assembly could be achieved without complicated trajectory planning.

I. INTRODUCTION

Many in-demand tasks in the field of automation are contact-rich tasks, i.e., those involving contact state transitions. In contact rich tasks, the mechanical constraints vary considerably with the transition of the contact state between the robot and environment. Thus, implementation of the control program becomes complex. Various studies have been conducted on contact-rich tasks using the assembly benchmark peg-in-hole (PiH) to expand the scope of automation technology [1]. In particular, assembly with a clearance of several microns, which is called precision assembly, requires accuracy exceeding the positional accuracy of the robot itself, making assembly using position control alone difficult. Robots are typically made compliant by control or a similar mechanism to conduct assembly without causing collisions due to positional errors. The former is called active compliance, and the latter is called passive compliance.

Impedance and admittance control are widely adopted as control methods that form the basis of active compliance [2]. Compliance control approaches generating assembly trajectories that satisfy the mechanical constraints of contact can be divided into contact-model-based and contact-model-free approaches [1]. The contact-model-based approach recognizes the contact state from the sensor information and calculates the appropriate assembly trajectory based on the contact model [3], [4]. The contact-model-free approach is a method that uses machine learning. Examples include a method called

learning from demonstration (LfD) that enables the robot to learn from demonstrations given by humans [5], [6], and a method called learning from the environment (LfE) that enables the robot to learn from the data on its state with respect to an environment [7]–[9]. Furthermore, hand stiffness is considered critical in research focusing on human motion control. Thus, to obtain useful information that can be extended to robotic motion control, research on estimating the stiffness of the human hand [11] is underway. Ajoudani *et al.* proposed a tele-impedance control method that uses an estimated value of human arm stiffness to control a robot and conduct PiH tasks [12]. Variable impedance control for online adaptation to environmental changes has also been actively studied [13].

Methods that use passive compliance obtain the desired stiffness of the hand by using a device that combines passive mechanical elements such as springs. The remote center compliance (RCC) device is one of the most popular examples, which utilizes the inter-axis interference to induce the motion against external force [14]. To deal with complicated tasks, variable RCC (VRCC), that can set stiffness in a variable manner, is being actively researched [15]. Lee proposed a VRCC device that operates using a rod that adjusts hand stiffness [16]. Drigalski *et al.* created a compliance hand with a wide adaptive error range to overcome the challenge of an error range narrowed by mechanical constraints [17]. Furthermore, Hamaya *et al.* proposed a supplemental method with path planning [18] and LfD [19].

Development of a mechanical design theory of RCC devices is an important challenge to eliminate posture interference due to environmental changes. Loncaric showed that a generic stiffness matrix can be transformed into a normal form in which rotational and translational aspects are maximally decoupled by a particular choice of the coordinate frame [20]. Roberts expanded on these results by showing that an arbitrary semi-fixed-value spatial stiffness matrix could be written in the regular form [21]. These design theories aim at eliminating the non-diagonal components of the stiffness matrix to suppress inter-axis interference.

Although the control system can be implemented easily and inexpensively using passive compliance, re-design or re-manufacturing are often needed for different tasks. Since active compliance methods are characterized by the ability to adjust settings arbitrarily, applying the RCC principle of inducing motion by adjusting stiffness to these methods would be beneficial. Oikawa *et al.* focused on the fact that inter-axis interference by non-diagonal elements in the stiffness matrix could be used for peg guidance and proposed a method of adjusting the stiffness matrix using reinforcement learning (RL) [22]. Kozlovsky *et al.* showed that the sample inefficiency of on-policy RL improves by reducing the action-space and simplifying the policy by learning asymmetric impedance

¹Tsukasa Kusakabe and Toshiaki Tsuji are with the Graduate School of Science and Engineering, Saitama University, 255 Shimo-okubo, Saitama, 338-8570 E-mail: tsuji@ees.saitama-u.ac.jp

²Sho Sakaino is with the Graduate School of Systems and Information Engineering, University of Tsukuba, 1-1-1 Tennodai, Tsukuba, Ibaraki 305-8577, Japan and the JST PRESTO

matrices [23]. Although some studies show the advantage of the use of non-diagonal elements, the design theory of the stiffness matrix remains unestablished. Therefore, in this study, we consider the design of the non-diagonal elements of the stiffness matrix, which are key to achieving motion guidance. Particularly, we focus on the fact that compliance control can use asymmetric matrices and show that the design of eigenvalues can be simplified by using a triangular matrix.

This approach expands the range of the non-diagonal elements of the stiffness matrix and enhances the ability of the compliance control to induce motion. We conduct experiments using the stiffness matrix and confirm that assembly can be achieved without complicated trajectory planning.

II. MOTION INDUCTION BASED ON COMPLIANCE CONTROL

We propose a method to design a control system using the following steps.

- 1) Specify the contact conditions that can occur in contact-rich tasks.
- 2) Design a path from all possible contact states to the goal contact state.
- 3) Generate a trajectory to transition to the next contact state toward the goal, and design a stiffness matrix suitable for that trajectory.

In this section, we first describe the use of non-diagonal terms of compliance control to induce motion, and then we explain basics of admittance control. After describing the design of a non-diagonal matrix assuming a symmetric matrix, we extend the method to the asymmetric case. We then discuss the advantage of a triangular matrix, and finally the implementation method for an actual PiH is described.

A. Path planning considering different contact states

Fig. 1 shows phases of the PiH in this study. For simplicity, an example is shown where both the cylindrical hole and the peg are perpendicular to the plate. After the peg contacts the surface, the phases can be divided into the search and insertion phase. Fig. 2 shows the force and moment in the search phase at the moment of contact with the environment. From Fig. 2, it can be seen that the sign of each moment τ_y and τ_x applied to the hand corresponds to the direction of the hole when an error is generated in each x and y direction, respectively. After an error has been generated, it is possible to guide the peg toward the hole by generating position displacement in response to the moment. Therefore, we consider the design of non-diagonal elements that induce the desired positional displacements $\Delta x_{desired}$ and $\Delta y_{desired}$ by τ_y and τ_x , respectively, and extend it to the asymmetrically arranged stiffness matrix.

B. Admittance control and its stiffness matrix

We adopt admittance control based on (1) for compliance control.

$$\mathbf{F}_{res} = M\Delta\ddot{\mathbf{X}}_{cmd}^{adm} + D\Delta\dot{\mathbf{X}}_{cmd}^{adm} + K\Delta\mathbf{X}_{cmd}^{adm} \quad (1)$$

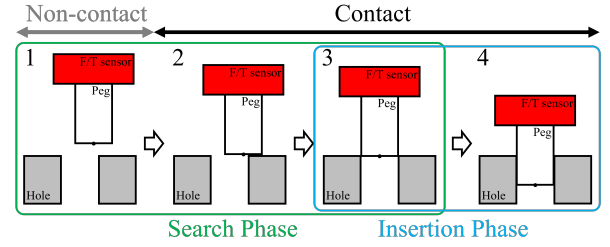


Fig. 1. Phases of peg-in-hole

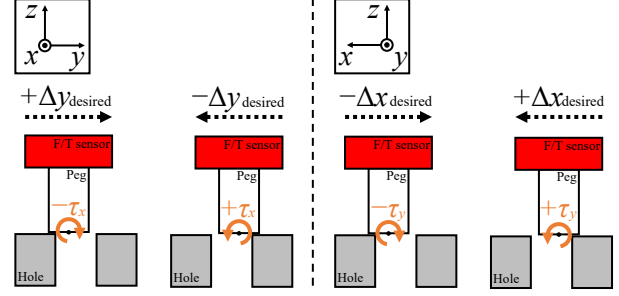


Fig. 2. Search phase of peg-in-hole

$$\mathbf{f} = \begin{bmatrix} f_x \\ f_y \\ f_z \end{bmatrix}, \quad \boldsymbol{\tau} = \begin{bmatrix} \tau_x \\ \tau_y \\ \tau_z \end{bmatrix}, \quad \mathbf{F}_{res} = \begin{bmatrix} \mathbf{f} \\ \boldsymbol{\tau} \end{bmatrix}$$

$$\Delta\mathbf{x} = \begin{bmatrix} \Delta x \\ \Delta y \\ \Delta z \end{bmatrix}, \quad \Delta\mathbf{r} = \begin{bmatrix} \Delta r_x \\ \Delta r_y \\ \Delta r_z \end{bmatrix}, \quad \Delta\mathbf{X}_{cmd}^{adm} = \begin{bmatrix} \Delta\mathbf{x} \\ \Delta\mathbf{r} \end{bmatrix}$$

Here, M , D and K denote mass, viscosity, and stiffness of the admittance model, respectively. f , m , and Δr denote force, moment, postural displacement, respectively. Δx , Δy and Δz denote positional displacement in the x , y , and z axis, respectively.

Fig. 3 shows a block diagram of the control system. The stiffness matrix, K , represents the static ratio of the displacement $\Delta\mathbf{x}$ and force/moment \mathbf{F} . K_p and K_v denote the proportional and derivative gain, respectively. \mathbf{J} and \mathbf{I} denote the Jacobian and inertia matrix, respectively. $\boldsymbol{\theta}_{res}$ denotes the joint angle response and \mathbf{X}_{cmd} denotes the position command. The methods described below are also applicable to impedance

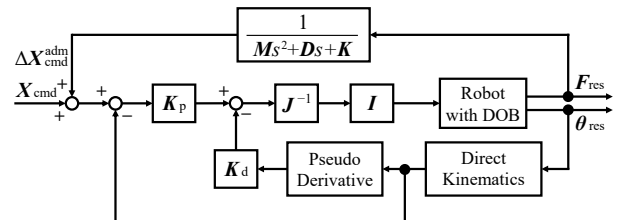


Fig. 3. Blockdiagram of admittance control.

control systems.

$$\mathbf{F} = \mathbf{K}\Delta\mathbf{X} \dots \dots \dots (2)$$

$$\begin{bmatrix} f_x \\ f_y \\ f_z \\ \tau_x \\ \tau_y \\ \tau_z \end{bmatrix} = \begin{bmatrix} k_{xx} & k_{xy} & k_{xz} & k_{xr_x} & k_{xr_y} & k_{xr_z} \\ k_{yx} & k_{yy} & k_{yz} & k_{yr_x} & k_{yr_y} & k_{yr_z} \\ k_{zx} & k_{zy} & k_{zz} & k_{zr_x} & k_{zr_y} & k_{zr_z} \\ k_{r_x x} & k_{r_x y} & k_{r_x z} & k_{r_x r_x} & k_{r_x r_y} & k_{r_x r_z} \\ k_{r_y x} & k_{r_y y} & k_{r_y z} & k_{r_y r_x} & k_{r_y r_y} & k_{r_y r_z} \\ k_{r_z x} & k_{r_z y} & k_{r_z z} & k_{r_z r_x} & k_{r_z r_y} & k_{r_z r_z} \end{bmatrix} \begin{bmatrix} \Delta x \\ \Delta y \\ \Delta z \\ \Delta r_x \\ \Delta r_y \\ \Delta r_z \end{bmatrix} (3)$$

Here, using the inverse matrix, \mathbf{K}^{-1} , the relationship is established as:

$$\Delta\mathbf{X} = \mathbf{K}^{-1}\mathbf{F} \dots \dots \dots (4)$$

$$\begin{bmatrix} \Delta x \\ \Delta y \\ \Delta z \\ \Delta r_x \\ \Delta r_y \\ \Delta r_z \end{bmatrix} = \begin{bmatrix} k_{xx}^{inv} & k_{xy}^{inv} & k_{xz}^{inv} & k_{xr_x}^{inv} & k_{xr_y}^{inv} & k_{xr_z}^{inv} \\ k_{yx}^{inv} & k_{yy}^{inv} & k_{yz}^{inv} & k_{yr_x}^{inv} & k_{yr_y}^{inv} & k_{yr_z}^{inv} \\ k_{zx}^{inv} & k_{zy}^{inv} & k_{zz}^{inv} & k_{zr_x}^{inv} & k_{zr_y}^{inv} & k_{zr_z}^{inv} \\ k_{r_x x}^{inv} & k_{r_x y}^{inv} & k_{r_x z}^{inv} & k_{r_x r_x}^{inv} & k_{r_x r_y}^{inv} & k_{r_x r_z}^{inv} \\ k_{r_y x}^{inv} & k_{r_y y}^{inv} & k_{r_y z}^{inv} & k_{r_y r_x}^{inv} & k_{r_y r_y}^{inv} & k_{r_y r_z}^{inv} \\ k_{r_z x}^{inv} & k_{r_z y}^{inv} & k_{r_z z}^{inv} & k_{r_z r_x}^{inv} & k_{r_z r_y}^{inv} & k_{r_z r_z}^{inv} \end{bmatrix} \begin{bmatrix} f_x \\ f_y \\ f_z \\ \tau_x \\ \tau_y \\ \tau_z \end{bmatrix} (5)$$

Compliance control achieves a compliance behavior for a tip defined at a single point on the end-effector. While the external force acting on the tip can be replaced by the external force of the sensor, there is a difference between the moment acting on the tip and the moment detected by the sensor in proportion to the distance between them, as shown in (7).

$$\mathbf{f}^{sensor} = \mathbf{f}^{peg} \dots \dots \dots (6)$$

$$\boldsymbol{\tau}^{sensor} = \boldsymbol{\tau}^{peg} + \mathbf{l}^e \mathbf{f}^{peg} \dots \dots \dots (7)$$

where the superscripts sensor and peg denote the sensor response and actual value on the tip of the peg, respectively. \mathbf{l}^e denotes the relative position from the sensor to the tip of the peg. Therefore, the moment on the tip should be calculated by the following formula:

$$\boldsymbol{\tau}^{peg} = \boldsymbol{\tau}^{sensor} - \mathbf{l}^e \mathbf{f}^{sensor} \dots \dots \dots (8)$$

If any external force acts on the tip, the formula cancels this error, but in practice the contact point moves depending on the motion of the robot. Therefore, in any compliance control method, the external force is considered to be acting on the tip, and the gain design is based on the assumption that errors due to fluctuations in the contact position will occur. In the PiH, the tip is defined as the center point of the bottom of the peg, since external forces are expected to mainly act on the bottom of the peg.

C. Design of symmetric stiffness matrix

In this subsection, we describe the properties of the diagonal and non-diagonal elements of the stiffness matrix and its inverse. First, a diagonal element k_{yy}^{inv} has the effect of inducing displacement Δy in the translational direction according to the force f_y applied in the translational direction. In other words, the diagonal elements of the stiffness matrix induce positional/postural displacement along the same axis as the applied force/moment. Similarly, non-diagonal elements $k_{yr_x}^{inv}$ of the stiffness matrix have the effect of inducing displacement Δy in the translational direction according to moment τ_x applied to the rotational direction. Thus, all the non-diagonal elements

of the stiffness matrix induce displacement along an axis that is different from the direction of the applied force/moment. The non-diagonal element values represent the amount of interference, and their arrangement determines which axis causes the interference. Although inter-axis interference can be manipulated by adjusting the values of each element, the system can be unstable depending on the parameter settings, unlike mechanical passive mechanisms. Therefore, focusing on the eigenvalues of the stiffness matrix, we designed the parameters so that divergent vibration modes do not occur.

Based on an energy function derived from a symmetric stiffness matrix, passivity of the admittance model can be ensured by setting the stiffness matrix to a definite-value symmetric matrix, as in the case of mechanical elastic structures [24]. For this to be the case, all eigenvalues λ of a matrix must be positive. For example, if the case of a two-dimensional stiffness matrix is expressed as

$$\begin{bmatrix} f_y \\ f_z \end{bmatrix} = \begin{bmatrix} k_{yy} & k_{yz} \\ k_{zy} & k_{zz} \end{bmatrix} \begin{bmatrix} \Delta y \\ \Delta z \end{bmatrix} = \begin{bmatrix} k_{yy} & k_n \\ k_n & k_{zz} \end{bmatrix} \begin{bmatrix} \Delta y \\ \Delta z \end{bmatrix} (9)$$

$$\begin{bmatrix} \Delta y \\ \Delta z \end{bmatrix} = \begin{bmatrix} k_{yy}^{inv} & k_{yz}^{inv} \\ k_{zy}^{inv} & k_{zz}^{inv} \end{bmatrix} \begin{bmatrix} f_y \\ f_z \end{bmatrix} = \begin{bmatrix} k_n^{inv} & k_{yy}^{inv} \\ k_{zz}^{inv} & k_n^{inv} \end{bmatrix} \begin{bmatrix} f_y \\ f_z \end{bmatrix} (10)$$

then its eigen equation is

$$(k_{yy} - \lambda)(k_{zz} - \lambda) - k_n^2 = 0. \dots \dots \dots (11)$$

Subsequently, the condition where the eigenvalues λ become positive can be determined as follows:

$$k_{yy}k_{zz} > k_n^2 \dots \dots \dots (12)$$

It is possible in principle to extend this to 6 dimensions and design parameters so that all eigenvalues are positive. However, as the number of parameters increases, the conditionals become more complex.

D. Asymmetrically arranged stiffness matrix design

As mentioned in the previous subsection, cases of symmetrical arrangements must satisfy the conditions of positive-definite symmetry. This indicates that when the stiffness matrix (which is a real symmetric matrix) is diagonalized, the eigenvalues of the stiffness matrix must be positive. However, it also means that the elastic energy generated by the displacement must always be positive. Moreover, the diagonalized matrix can be considered as the stiffness on each co-axis. Thus, the stiffness matrix with symmetrically arranged non-diagonal elements represents the distribution where the stiffness in each axis is rotated arbitrarily, known as the stiffness ellipse. Even in the case of asymmetrically arranged non-diagonal elements, the eigenvalues of the stiffness matrix, which are related to the square of the modal frequencies [25], must be positive. Here, as an example, we determine the conditions to be satisfied by asymmetric stiffness matrix \mathbf{K} for a two-dimensional space (yz plane).

$$\mathbf{K} = \begin{bmatrix} k_{yy} & k_{yz} \\ k_{zy} & k_{zz} \end{bmatrix} = \begin{bmatrix} k_{yy} & k_{yz} \\ 0 & k_{zz} \end{bmatrix} \dots \dots \dots (13)$$

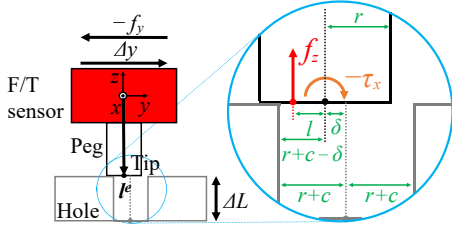


Fig. 4. Peg-in-hole (interference in +y-axis). Variables: radius of peg (r), clearance (c), distance between centers of hole and peg (δ), depth of position command (ΔL), friction coefficient (μ), and distance between the center of peg and the center of pressure (l)

is set, and the relationship with the external force F and the positional displacement ΔX is expressed as follows:

$$\begin{bmatrix} f_y \\ f_z \end{bmatrix} = \begin{bmatrix} k_{yy} & k_{yz} \\ 0 & k_{zz} \end{bmatrix} \begin{bmatrix} \Delta y \\ \Delta z \end{bmatrix} \quad \dots \quad (14)$$

$$\begin{bmatrix} \Delta y \\ \Delta z \end{bmatrix} = \begin{bmatrix} k_{yy}^{inv} & k_{yz}^{inv} \\ 0 & k_{zz}^{inv} \end{bmatrix} \begin{bmatrix} f_y \\ f_z \end{bmatrix} \quad \dots \quad (15)$$

From (14) and (15), the external force f_y only changes displacement Δy in the y -direction, whereas external force f_z induces a displacement in both Δy and Δz . Thus, when arranging the stiffness matrix asymmetrically in a triangular matrix, only specific axes will interfere unilaterally.

The conditions where the eigenvalues become positive are as follows:

$$k_{yy} > 0 \wedge k_{zz} > 0. \quad \dots \quad (16)$$

It is known that the eigenvalues of a triangular matrix coincide with the diagonal components of the matrix. Therefore, when (16) is extended to 6 dimensions, the conditions are obtained as follows:

$$k_{xx} > 0 \wedge k_{yy} > 0 \wedge k_{zz} > 0 \wedge k_{r_x r_x} > 0 \wedge k_{r_y r_y} > 0 \wedge k_{r_z r_z} > 0. \quad \dots \quad (17)$$

There are no theoretical constraints on the non-diagonal components because they do not affect the eigenvalues.

It should be noted here that the elastic energy of the asymmetrical stiffness matrix cannot be determined in the same manner as that for a symmetrical stiffness matrix. This is because an asymmetrical stiffness matrix is not a positive-definite symmetric matrix and it does not satisfy the Maxwell-Betti reciprocal work theorem, which states that the spring arrangement must cause equivalent interference on the axes.

Furthermore, the determinant $\det(\mathbf{K})$ is always positive when the matrix is inverted, which shows the ease of design. Thus, the non-diagonal elements have a larger range of values compared with the symmetrical matrices and the configurable range of the stiffness matrix expands.

E. Task-specific design of stiffness matrix

In this subsection, we describe a method for designing non-diagonal elements that conduct a PiH task as one typical example. Based on the discussions in the previous subsections, a triangular matrix is adopted because it expands the range

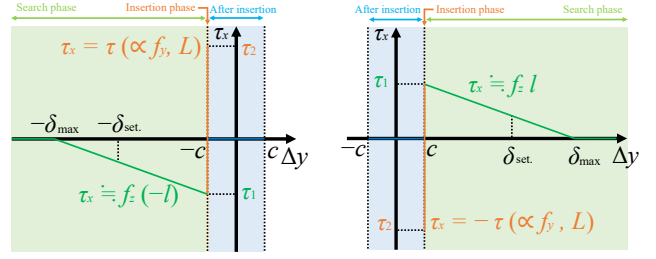


Fig. 5. Relation between τ_x and δ_x in negative region Fig. 6. Relation between τ_x and δ_x in positive region

over which all eigenvalues are positive and simplifies the design. Fig. 4 shows a schematic of the PiH task in a three-dimensional space during the search. This figure shows that the contact position changes depending on the displacement Δy and that the sign of the moment τ_x should also change accordingly. Then, an effective design on a non-diagonal element $k_{y r_x}$ would induce displacements Δy . In the same token, $k_{x r_y}$ would also induce displacements Δx . To design $k_{x r_y}$ and $k_{y r_x}$, first, we consider the contact position of Fig. 4. Since $c \ll |\delta|$, we set $|\delta| - c \doteq |\delta|$. The amount of interference by the non-diagonal elements is expressed as follows:

$$\delta = k_{yy}^{inv} f_y + k_{y r_x}^{inv} \tau_x \quad \dots \quad (18)$$

Here, k_{yy}^{inv} is considered, in addition to $k_{y r_x}^{inv}$, because the external force on y -axis directly interferes with the movement in y -axis. Conversely, other non-diagonal elements are not considered because they do not have a direct relationship to the movement in the y -axis.

Substituting $f_y = -\mu f_z$ and $\tau_x = -f_z l$ to (20),

$$\delta = -\mu k_{yy}^{inv} f_z + k_{y r_x}^{inv} l f_z \quad \dots \quad (19)$$

Here, the position command is set ΔL below the top surface to obtain a constant contact force f_z during the search phase. Assuming $f_z = \Delta L k_{zz}^{inv}$, the following is obtained:

$$\delta = -\frac{(\mu k_{yy}^{inv} + k_{y r_x}^{inv}) \Delta L}{k_{zz}^{inv}} \quad \dots \quad (20)$$

where $k_{y r_x}^{inv}$, which is a non-diagonal element that is to be obtained, can be expressed as follows by substituting $\mu = 0$ into (20). In the same token, $k_{x r_y}$ can also be derived:

$$k_{y r_x}^{inv} = k_{x r_y}^{inv} = -\frac{\delta_{set} k_{zz}^{inv}}{l_{set} \Delta L} \quad \dots \quad (21)$$

Here, δ_{set} denotes the maximum possible error and l_{set} denotes the distance to the center of pressure when the maximum possible error occurs.

By setting up the non-diagonal element using (21), the deviation δ_{set} is generated when the peg is not inserted, despite the command beneath the top surface. The parameters of the stiffness matrix should be changed depending on the task and contact state during the task. Since the tip of the peg is set as the compliance center in this study, errors may occur when the contact point is away from the compliance center, depending on the interference of translational forces f_x and f_y and moments τ_x and τ_y .

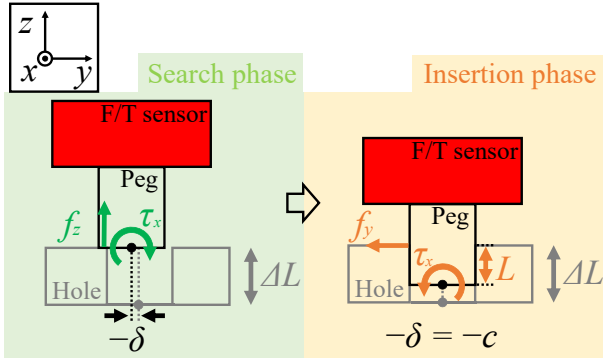


Fig. 7. Force and torque during search and insertion phases

The contact position and force in each axis fluctuate discontinuously as the contact states change. The errors described above also occur in proportion to the magnitude of the contact position variation. Even if the compliance control is designed to be passive, hunting occurs due to these factors. As mentioned in the previous section, there is no theoretical restriction on the non-diagonal elements that make the eigenvalues of the triangular matrix positive. However, to avoid hunting, this error must be assumed, and this gives a substantial constraint in the setting of the non-diagonal elements. If the maximum force error expected for the task is estimated, substituting the maximum force into (20) yields the maximum width of the hunting movement. It is necessary to set the non-diagonal elements so that the hunting width is within acceptable limits.

III. EXPERIMENT

A. Experimental device setup

We conducted experimental evaluations using a real robot. Simulations based on the parameters of the actual machine were also used to evaluate quantitative comparisons from a safety perspective. Both used an industrial six-axis manipulator, and a six-axis force sensor was attached to the wrist of the robot. Fig. 8 shows the manipulator used in the simulation, the coordinate system, and the manipulator used in the real robot. Table I presents the specifications of the manipulator used in the real robot. The manipulator used in the simulation had the same parameters as the experimental device. Table II lists each control parameter.

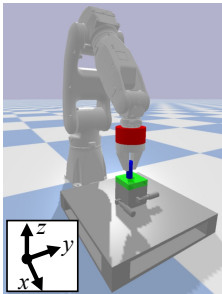


Fig. 8. Simulation setup

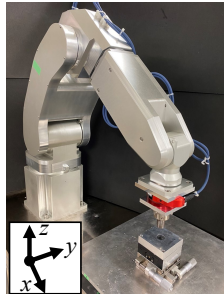


Fig. 9. Experimental setup

TABLE I
SPECIFICATIONS OF MANIPULATOR

	Max. torque [Nm]	Max. velocity [rad/s]	Link length from previous joint [mm]
Joint 1	68.5	1.70	200
Joint 2	73.0	1.59	130
Joint 3	27.5	2.12	345
Joint 4	12.9	2.26	100
Joint 5	11.0	2.65	240
Joint 6	7.4	4.56	80

TABLE II
CONTROL PARAMETERS

Proportional gain	K_p	diag[600, 600, 600, 600, 600, 600]
Derivative gain	K_d	diag[50.0, 50.0, 50.0, 50.0, 50.0, 50.0]
Moment of inertia [kgm ²]	I	diag[2.0, 1.0, 0.8, 0.25, 0.15, 0.05]
Mass of admittance model [kg]	M	diag[1.0, 1.0, 1.0, 1.0, 1.0, 1.0]
Damper of admittance model [Ns/m]	D	diag[50.0, 50.0, 50.0, 5.0, 5.0, 5.0]
Cutoff frequency of derivative filter [Hz]	g	1.5
Sampling time [s]	T_s	0.001

B. Simulation stability comparison

First, we evaluated the performance of the proposed method by simulating the induction by stiffness ellipses without limitation of maximum external force. We compared the inductive effect of the proposed method with an asymmetric matrix to that of a symmetric matrix. A vertical command trajectory on the z-axis was given with the maximum command depth $\Delta L = 20[\text{mm}]$. Then the robot with a 20 mm diameter peg made contact with the top surface of the plate and the motion was induced in the y-axis after contact. Here, the friction coefficient μ was 0.4.

Fig. 10 shows the simulation results using symmetric matrices. Here, K_{d20} and K_{d30} denote the symmetric matrices designed to induce the motion in the y-axis with 20 mm and 30 mm lengths, respectively. The results in Fig. 10 show that the motion was induced in the desired direction with the use of K_{d20} , but no significant increase in the response values was observed with the use of K_{d30} . This is because the inclination of the stiffness ellipse decreases as the amount of interference increases, and the force acts along the direction close to the long-axis direction of the inclined stiffness ellipse due to the frictional force. In the stiffness matrices designed for induction above 30 mm, the inductive effect in the y-axis no longer occurred due to this effect.

Meanwhile, the results in Fig. 11 show that the interference in the response values were generally in proportion to the design values of the four interferences (20, 30, 60, and 120 mm). Here, the stiffness matrices were designed as follows:

$$K_{n20} = \begin{bmatrix} 500 & -500 \\ 0 & 750 \end{bmatrix}, K_{n30} = \begin{bmatrix} 500 & -750 \\ 0 & 750 \end{bmatrix}$$

$$K_{n60} = \begin{bmatrix} 500 & -1500 \\ 0 & 750 \end{bmatrix}, K_{n120} = \begin{bmatrix} 500 & -3000 \\ 0 & 750 \end{bmatrix}$$

In all cases, the response values were slightly below the design values due to friction in the sliding direction. This is

a reasonable result because the robot reproduces the desired impedance and the same phenomenon occurs with RCC, which sets the impedance mechanically.

As shown in Fig. 11, the asymmetrical arrangement induces interference in the y-axis at the desired force of $f_z = 15$ N. The amount of interference depends on the friction coefficient of the member, regardless of whether it is symmetrical or asymmetrical. The asymmetrical arrangement enables contact with the desired force; furthermore, the non-diagonal elements can assume a wider range of values when compared with the symmetrical arrangement. Therefore, in asymmetrically arranged matrices, the value of interference with other axes is less constrained than in symmetrically arranged matrices.

C. Experimental result

The stiffness matrix was designed as follows:

$$K = \begin{bmatrix} 500 & 0 & 0 & 0 & k_{xry} & 0 \\ 0 & 500 & 0 & k_{yrx} & 0 & 0 \\ 0 & 0 & 500 & 0 & 0 & 0 \\ 0 & 0 & 0 & 50 & 0 & 0 \\ 0 & 0 & 0 & 0 & 50 & 0 \\ 0 & 0 & 0 & 0 & 0 & 50 \end{bmatrix} \quad (22)$$

Assuming that an error of ± 5 mm would be generated in each direction of the x- and y-axes, we designed k_{xry} and k_{yrx} using (21), and conducted PiH with a 30-mm diameter (clearance of $420 \mu\text{m}$) and 20-mm diameter (clearance of $40 \mu\text{m}$) peg. Fig. 12 shows the number of successes and failures for different positional errors. The experiments show that the proposed method has the ability to perform PiH via adjustment of the stiffness matrix and without environment-adaptive trajectory planning. RCC, which also performs PiH with only stiffness adjustment, was employed as a baseline method. In this experiment, however, the behavior was reproduced, not by the mechanism, but by the control. For the 30-mm diameter ($420 \mu\text{m}$ clearance), all locations resulted in successful insertion for five out of five attempts; and for the 20-mm diameter ($40 \mu\text{m}$ clearance), all but two locations resulted in task completion.

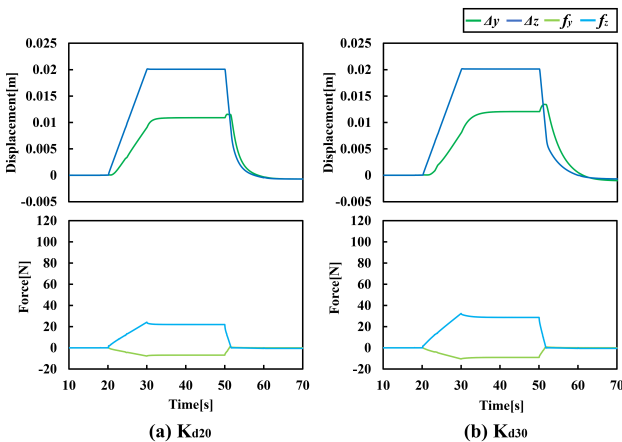


Fig. 10. Responses with each stiffness matrix with different interference design. (symmetric)

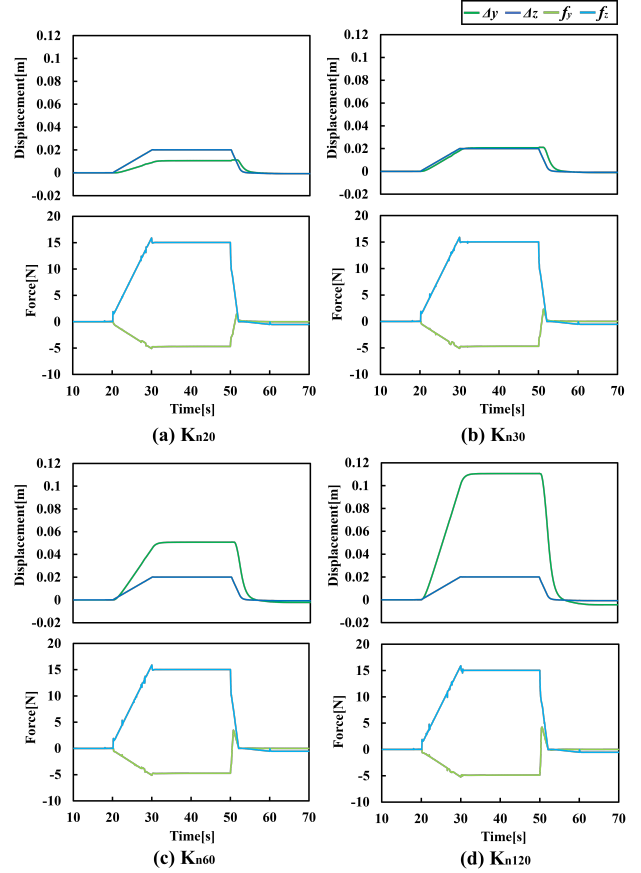


Fig. 11. Responses with each stiffness matrix with different interference design. (asymmetric)

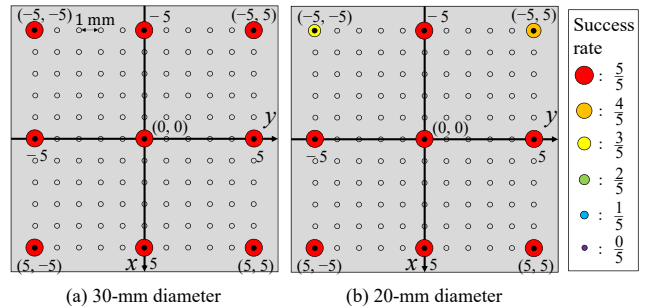


Fig. 12. Success rate of PiH experiment

The results of implementing the same design as the RCC in an admittance control are shown in Fig. 13. The success rates were evaluated over a sufficiently long time for insertion to ensure that implementation by control, rather than mechanism, would not lower the evaluation. In general, RCCs are designed to passively displace only its position, without changing its posture, in response to external forces in the insertion direction. Therefore, the position error of the peg is compensated by the contact force from the edge of the hole acting in the direction of the center of the hole. However, if the error is large, the external force from the edge of the hole will not guide the peg to the direction of the hole, and the error correction range will be limited. In contrast, the proposed

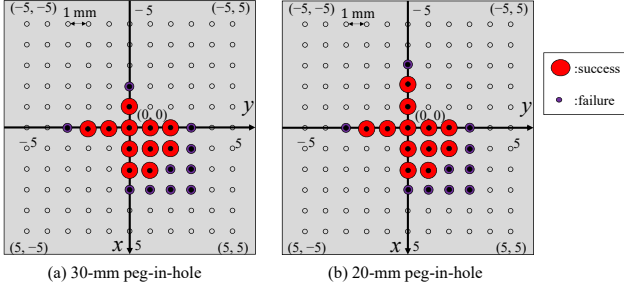


Fig. 13. PiH experiment of the baseline method

method designs the non-diagonal component to guide the peg in the direction of the hole according to the moment. Therefore, the position error was compensated for even when the error was larger. In other words, it was confirmed that the error tolerance of PiH can be expanded by extending the setting range of the stiffness matrix to a region that has not been considered in the past.

Next, the positional displacement command and force value determined at each axis by the stiffness matrix at an error of $\Delta(x, y) = (-5, -5)$ for a 20-mm diameter PiH are shown in Fig. 14. It can be seen from the results around time 30 [s] that contact with the hole edge results in the application of a force f_z in the insertion direction. This generates τ_y and τ_x according to its magnitude. Finally, these moments interfere with Δy and Δx , respectively, due to the non-diagonal elements. Compared with the PiH of the 30-mm case, the 20-mm diameter peg had a narrower clearance and an environment where the moment was less likely to occur. For this reason, there was one failure out of five for the $\Delta(x, y) = (-5, 5)$ case and two failures out of five for the $\Delta(x, y) = (-5, -5)$ case. Nevertheless, all the pegs were inserted in a stable manner in the areas where the error was small.

Fig. 15 shows the time required for insertion. For both the 30-mm and 20-mm diameter pegs, insertion was achieved with less variation and in a shorter time for an error of 5 mm compared with an error of $5\sqrt{2}$ mm. This is because the distance to the hole increased when the error increased to $5\sqrt{2}$ mm. Thus, more time was required for task completion. Furthermore, at the increased error level, it was difficult to generate a moment with the contact position due to the errors generated along both the x- and y-axes. In comparison, the insertion of the 20-mm diameter peg exhibited less variation and a shorter average time than the 30-mm diameter peg. In this experiment, the stiffness matrix was designed on the assumption that the friction coefficient was zero. Therefore, the frictional force became a source of error, but a larger effect was present in the case of the 30-mm diameter peg, which had a larger contact surface area than that of the 20-mm diameter peg.

IV. CONCLUSION

In this study, we proposed a method for designing non-diagonal elements in a stiffness matrix. We described the extent to which non-diagonal elements that achieve the desired

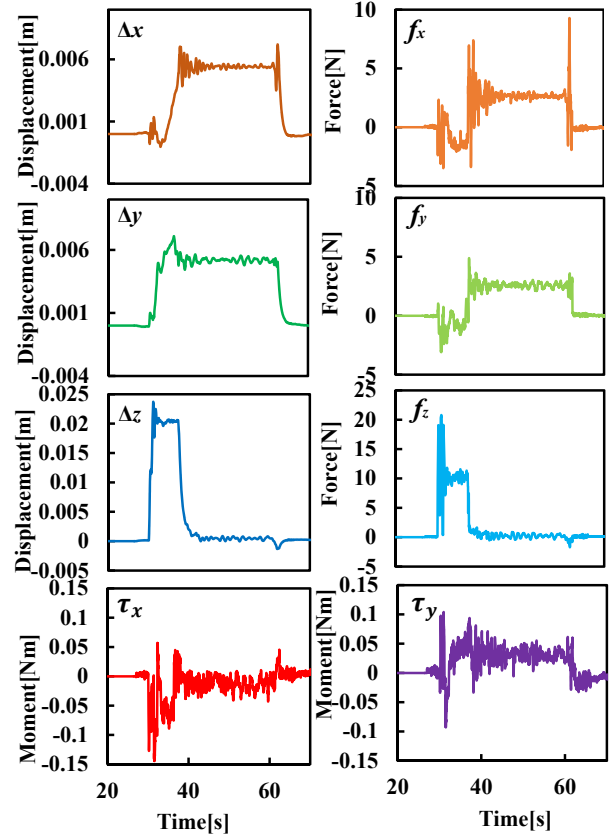


Fig. 14. Responses during insertion of 20-mm diameter peg

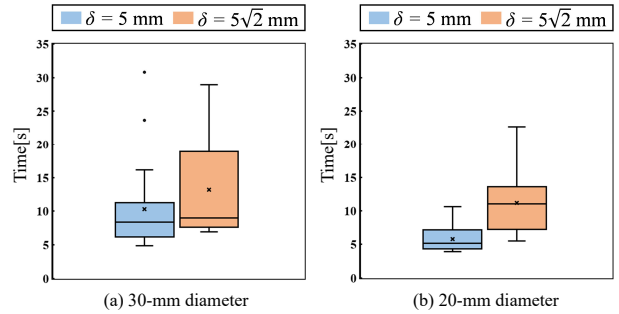


Fig. 15. Insertion time of PiH experiment

amount of interference could be designed, and the cases of symmetrical and asymmetrical arrangements. To obtain stable contact with a symmetric matrix, the matrix should be positive definite, i.e., all eigenvalues must be positive, however its parameter design is complicated. In this study, we therefore focused on the use of asymmetric matrices in compliance control and showed that the design of eigenvalues can be simplified by using a triangular matrix. This approach expands the range of the stiffness design and enhances the ability of the compliance control to induce motion. The experiments using the stiffness matrix based on the proposed method, demonstrated that assembly is possible with just a simple trajectory. In addition, it showed that precision assembly with a clearance of several dozens of microns is possible.

REFERENCES

- [1] J. Xu, Z. Hou, Z. Liu, and H. Qiao: "Compare contact model-based control and contact model-free learning: A survey of robotic peg-in-hole assembly strategies," *arXiv preprint, 1904.05240*, 2019.
- [2] N. Hogan: "Impedance control: An approach to manipulation," in *Proceedings of American Control Conference (ACC)*, pp. 304–313, 1984.
- [3] H. Qiao, M. Wang, J. Su, S. Jia, and R. Li: "The concept of "attractive region in environment" and its application in high-precision tasks with low-precision systems," *IEEE/ASME Trans. on Mechatronics*, vol. 20, no. 5, pp. 2311–2327, 2015.
- [4] T. Tang, H. Lin, Y. Zhao, W. Chen, and M. Tomizuka: "Autonomous alignment of peg and hole by force/torque measurement for robotic assembly," in *Proc. 2016 IEEE Int. Conf. on Automation Science and Engineering (CASE)*, pp. 162–167, 2016.
- [5] S. Schaal: "Learning from demonstration," in *Proceedings of Advances in Neural Information Processing Systems (NIPS)*, vol. 9, 1997.
- [6] S. Gubbi, S. Kolathaya, and B. Amrutur: "Imitation learning for high precision peg-in-hole tasks," in *Proceedings of 6th International Conference on Control, Automation and Robotics (ICCAR)*, pp. 368–372, 2020.
- [7] J. Luo, E. Solowjow, C. Wen, J. A. Ojea, A. M. Agogino, A. Tamar, and P. Abbeel: "Reinforcement learning on variable impedance controller for high-precision robotic assembly," in *Proceedings of International Conference on Robotics and Automation (ICRA)*, pp. 3080–3087, 2019.
- [8] T. Inoue, G. D. Magistris, A. Munawar, T. Yokoya, and R. Tachibana: "Deep reinforcement learning for high precision assembly tasks," in *Proceedings of IEEE/RSJ International Conference on Intelligent Robots and Systems (IROS)*, pp. 819–825, 2017.
- [9] C. C. Beltran-Hernandez, D. Petit, I. G. Ramirez-Alpizar, and K. Harada: "Variable compliance control for robotic peg-in-hole assembly: A deep-reinforcement-learning approach," *Applied Sciences*, vol. 10, no. 19, pp. 6923, 2020.
- [10] O. Kroemer, S. Niekum, Konidaris, and G. D.: "A review of robot learning for manipulation: Challenges, representations, and algorithms," *Journal of machine learning research*, vol. 22, no. 30, 2021.
- [11] S. Wang, G. Zuo, J. Xu, and H. Zheng: "Human hand impedance characteristics during reaching movements," in *Proceedings of 4th International Conference on Biomedical Engineering and Informatics (BMEI)*, vol. 3, pp. 1282–1286, 2011.
- [12] A. Ajoudani, N. G. Tsagarakis, and A. Bicchi: "Tele-impedance: Preliminary results on measuring and replicating human arm impedance in tele operated robots," in *Proceedings of IEEE International Conference on Robotics and Biomimetics (ROBIO)*, pp. 216–222, 2011.
- [13] C. C. Beltran-Hernandez, D. Petit, I. G. Ramirez-Alpizar, T. Nishi, S. Kikuchi, T. Matsubara, and K. Harada: "Learning force control for contact-rich manipulation tasks with rigid position-controlled robots," *IEEE Robotics and Automation Letters*, vol. 5, no. 4, pp. 5709–5716, 2020.
- [14] D. E. Whitney: "Quasi-static assembly of compliantly supported rigid parts," *Journal of Dynamic Systems Measurement and Control-Transactions of the Asme*, vol. 104, pp. 65–77, 1982.
- [15] F. Zhao and P. S. Y. Wu: "VRCC : a variable remote center compliance device," *Mechatronics*, vol. 8, no. 6, pp. 657–672, 1998.
- [16] S. Lee: "Development of a new variable remote center compliance (VRCC) with modified elastomer shear pad (ESP) for robot assembly," *IEEE Transactions on Automation Science and Engineering*, vol. 2, pp. 193–197, 2005.
- [17] F. V. Drigalski, K. Tanaka, M. Hamaya, R. Lee, C. Nakashima, Y. Shibata, and Y. Ijiri: "A compact, cable-driven, activatable soft wrist with six degrees of freedom for assembly tasks," in *Proceedings of IEEE/RSJ International Conference on Intelligent Robots and Systems (IROS)*, pp. 8752–8757, 2020.
- [18] M. Hamaya, R. Lee, K. Tanaka, F. V. Drigalski, C. Nakashima, Y. Shibata, and Y. Ijiri: "Learning robotic assembly tasks with lower dimensional systems by leveraging physical softness and environmental constraints," in *Proceedings of IEEE International Conference on Robotics and Automation (ICRA)*, pp. 7747–7753, 2020.
- [19] M. Hamaya, F. V. Drigalski, T. Matsubara, K. Tanaka, R. Lee, C. Nakashima, Y. Shibata, and Y. Ijiri: "Learning soft robotic assembly strategies from successful and failed demonstrations," in *Proceedings of IEEE/RSJ International Conference on Intelligent Robots and Systems (IROS)*, pp. 8309–8315, 2020.
- [20] J. Loncaric: "Normal forms of stiffness and compliance matrices," *IEEE Journal on Robotics and Automation*, vol. 3, no. 6, pp. 567–572, 1987.
- [21] R. G. Roberts: "Note on the normal form of a spatial stiffness matrix," *IEEE Transactions on Robotics and Automation*, vol. 17, no. 6, pp. 968–972, 2001.
- [22] M. Oikawa, T. Kusakabe, K. Kutsuzawa, S. Sakaino, and T. Tsuji: "Reinforcement learning for robotic assembly using non-diagonal stiffness matrix," *IEEE Robotics and Automation Letters*, vol. 6, no. 2, pp. 2737–2744, 2021.
- [23] S. Kozlovsky, E. Newman, and M. Zacksenhouse, "Reinforcement Learning of Impedance Policies for Peg-in-Hole Tasks: Role of Asymmetric Matrices," *IEEE Robotics and Automation Letters*, vol. 7, no. 4, pp. 10898–10905, 2022.
- [24] T. Kusakabe, S. Sakaino, and T. Tsuji: "A Design Method for Non-Diagonal Stiffness Matrix in Admittance Control," *Int. Conf. on Control, Automation and Systems (ICCAS2021)*, FA9-3, P00161, 2021.
- [25] S. W. Doebeling, L. D. Peterson, and K. F. Alvin. "Experimental determination of local structural stiffness by disassembly of measured flexibility matrices." *J. Vib. Acoust.*, vol. 120, no. 4, pp. 949–957, 1998.